

Exciton–plasmon interactions in molecular spring assemblies of nanowires and wavelength-based protein detection

JAEBEOM LEE^{1,2}, PEDRO HERNANDEZ³, JUNGWOO LEE¹, ALEXANDER O. GOVOROV^{3*} AND NICHOLAS A. KOTOV^{1*}

¹Department of Chemical Engineering, Materials Science and Engineering, and Biomedical Engineering, University of Michigan, Ann Arbor, Michigan 48109, USA

²Department of Nanomedical Engineering, Pusan National University, Busan 609-735, Korea

³Department of Physics and Astronomy, Ohio University, Athens, Ohio 45701, USA

*e-mail: govorov@ohiou.edu; kotov@umich.edu

Published online: 25 March 2007; doi:10.1038/nmat1869

Electronic interactions at the nanoscale represent one of the fundamental problems of nanotechnology. Excitons and plasmons are the two most typical excited states of nanostructures, which have been shown to produce coupled electronic systems^{1–11}. Here, we explore these interactions for the case of nanowires with mobile excitons and nanoparticles with localized plasmons and describe the theoretical formalism, its experimental validation and the potential practical applications of such nanoscale systems. Theory predicts that emission of coupled excitations in nanowires with variable electronic confinement is stronger, shorter and blue-shifted. These predictions were confirmed with a high degree of accuracy in molecular spring assemblies of CdTe nanowires and Au nanoparticles, where we can reversibly change the distance between the exciton and the plasmon. The prepared systems were made protein-sensitive by incorporating antibodies in the molecular springs. Modulation of exciton–plasmon interactions can serve as a wavelength-based biodetection tool, which can resolve difficulties in the quantification of luminescence intensity for complex media and optical pathways.

When (bio)polymers and nanoparticles are combined in a superstructure, unique functionalities become possible because the physical properties of inorganic nanomaterials and the chemical flexibility/specificity of polymers can be used. Of particular interest are the complex systems combining two types of excitations common in nanomaterials, such as excitons and plasmons leading to coupled excitations^{7,8,10–12}, which are quite different from interactions between plasmons and excitations in dye molecules^{13–15}. Even considering recent successes in plasmonics^{16–22}, the fundamental description of such systems, methods for their structural control, as well as their practical functionalities represent a largely virgin scientific terrain.

Sensing functionalities are probably the most needed ones and constitute a perpetual technological challenge. The detection of analytes on the basis of variations of intensity as a transduction mechanism is the most successful and dominant technology in optical sensing and imaging. At the same time, technologies relying on variations of emission also have well-known problems: (1) intensity variations due to the presence of analyte and

local concentration variations of the luminescence label cannot be distinguished; (2) scattering properties of the sample can strongly affect the intensity readings; (3) the absolute reading of emission intensity depends on the light-collecting path in the registration system, which may vary from one set-up to another and can also be time dependent. All of these present problems for quantitative analysis and constitute the reasons why remote detection and biosensing have many difficulties when using intensity as an analytical parameter (see the Supplementary Information). In this paper, we introduce a new superstructure of CdTe nanowires (NWs) and Au nanoparticles (NPs) connected by molecular springs, which makes the first step towards a different approach to sensing by monitoring changes in the luminescence emission wavelength as a transduction mechanism. It also unravels the electronic mechanism of the underlying exciton–plasmon interactions in the presence of dynamic exciton behaviour, which can serve as a foundation for the future development of nanoscale superstructures with sensing and other functionalities.

Molecular spring assemblies (MSAs) made from Au and CdTe NPs, where the latter form a corona-like superstructure, have been demonstrated to have reversible variations in the intensity of excitonic CdTe luminescence on cycling the media²³ or temperature^{24,25}. Keeping the same design principle, we used NWs as the basic building blocks of the superstructure, which theoretically makes reversible wavelength shift sensing and imaging possible. Reversible wavelength shifts were investigated using a model based on the exciton–plasmon interactions in NWs surrounded by metallic NPs (Fig. 1a), which is analogous to the structures made previously^{24,25}.

Excitons inside the NW drift and diffuse in the presence of a non-uniform potential, arising, for example, from the variance in the NW diameter. For diameter variations, which are always present in the NWs, the originally generated exciton will emit a photon at lower energy after diffusion, it will eventually become preferentially located in the regions of smaller exciton energy (that is, a bandgap). These regions are usually formed because of spontaneous variations in the NW materials or dimensional characteristics, but may also be specifically engineered. How far an exciton can diffuse depends on its lifetime, τ_{exc} , which, in turn, depends on the intrinsic exciton

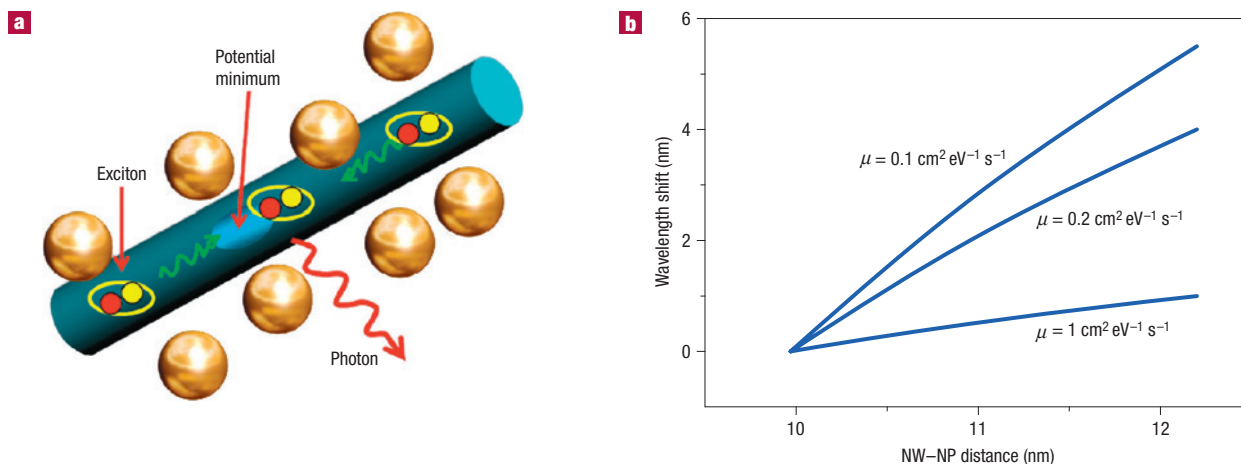


Figure 1 Theoretical model and results for exciton dynamic calculations in the nanowire assemblies with Au nanoparticles. **a**, Schematic diagrams of the system and physical processes. Excitons drift and diffuse towards the potential minima where they recombine. This leads to red-shifted emission. **b**, Calculated wavelength shift of exciton emission as a function of the NW-NP distance for the specified exciton mobilities.

recombination rate γ_0 in NWs and on the exciton-to-NP energy transfer rate γ_{NP} , as

$$\tau_{exc} = 1/(\gamma_0 + \gamma_{NP}). \quad (1)$$

γ_{NP} is very sensitive to the structural changes and in particular, to the NW-NP distance, R_{NW-NP} . Because of the similar dipole-dipole interaction mechanism in exciton-plasmon coupling and classical resonance energy transfer, γ_{NP} can be approximated using the Förster formula:

$$\gamma_{NP}(R_{NW-NP}) = \gamma_1 (R_0/R_{NW-NP})^6, \quad (2)$$

where γ_1 and R_0 are constants characteristic for nanoscale structures (see the Supplementary Information). Now, let us assume that there is a certain transduction mechanism for an analyte concentration or a periodic stimulus that changes the NW-NP distance. When the NW-NP distance decreases, the exciton lifetime decreases and not all excitons can reach the potential minima; this process leads to a chemically controllable blue exciton emission shift. The entire model described above can be formulated mathematically using the exciton-transport equations that involve equations (1) and (2) (see the Supplementary Information). Finally, we can obtain an equation connecting the emission spectrum to the exciton transfer rate and thus to $1/R_{NW-NP}$.

It is instructive to estimate the exciton wavelength shift for a reasonable change in R_{NW-NP} . On the basis of previous data²⁵, we use MSA structures comprising a poly(ethyleneglycol) (PEG) backbone with biological functionalities because we are interested in biosensing capabilities. These functionalities can be acquired by incorporating an antibody (aB) into the PEG chain as PEG-aB-PEG. Such structures can be made following standard bioconjugation protocols (see the Supplementary Information). We measured the hydrodynamic diameter of PEGylated anti-streptavidin (SA) aB when it reacted with the antigen (aG) to obtain a reasonable estimate for the change in R_{NW-NP} : it increased from 9.97 to 12.2 nm (see the Supplementary Information), which was attributed to a change in PEG conformation, and can be described as an extension of the

molecular springs. For the same system, the NW exciton lifetime $\tau_{exc}^0 = 1/\gamma_0$ was measured as $9 \text{ ns} \pm 1 \text{ ns}$ (ref. 12). From our optical experiments with Au-conjugated NWs, we know that the presence of Au NPs can dramatically change the exciton lifetime. After the formation of Au-PEG-aB-NW complexes with $R_{NW-NP} = 9.97 \text{ nm}$, $\tau_{exc} = 1/(\gamma_0 + \gamma_{NP})$ becomes $1 \pm 0.5 \text{ ns}$. Then, using this number and equation (2), we can estimate the constants in equation (2): $\gamma_1 = 1 \text{ ns}^{-1}$ and $R_0 = 9.97 \text{ nm}$. When R_{NW-NP} changes from 9.97 to 12.2 nm, the energy transfer rate and the total lifetime vary as follows: $0.3 \text{ ns}^{-1} < \gamma_{NP} < 1 \text{ ns}^{-1}$ and $0.9 \text{ ns} < \tau_{exc} < 2.45 \text{ ns}$.

With the parameters described in the Supplementary Information for the exciton diffusion model developed, it can be seen that the above change in R_{NW-NP} can create a noticeable emission wavelength shift (Fig. 1b). The actual magnitude of the shift will depend on the exciton mobility, μ , which is difficult to determine independently, in part because it is strongly affected by the quality of the NW (interface fluctuations) and potentially by the media (electrical field fluctuations from the solvent and ions). To establish the range of potential wavelength shift, we developed a model on the basis of the strong coupling of excitons in NW to plasmons in metal NPs²⁶. Note that we could also consider the plasmon enhancement of the photonic fields inside the NW due to clustering of metallic particles. However, as will be seen below and according to calculations given in the Supplementary Information, this effect is weak for structures with a relatively small linear density of Au NPs^{12,26}. The cumulative results of the wavelength shifts for different values of μ are shown in Fig. 1b and can be observed experimentally.

The structure described in Fig. 2a is suitable for the experimental validation of the wavelength-shift concept in NW-NP systems. The general strategy in the preparation of this MSA is to use linear bifunctional PEG oligomers (MW = 3,400 daltons) with *N*-hydroxy-sulphosuccinimide (NHS) and *t*-butoxycarbonyl (*t*-BOC) groups, in which only one specific terminal is reactive in a particular reaction. In this way, the degree of multi-NW crosslinking leading to precipitation is minimized and the yield of the desirable MSA is maximized. NHS is a suitable crosslinking group for making bonds to amines on NP/NW surfaces. The other terminal is a blocking group, *t*-BOC, which can be removed by trifluoric acid when a carboxylic group is needed

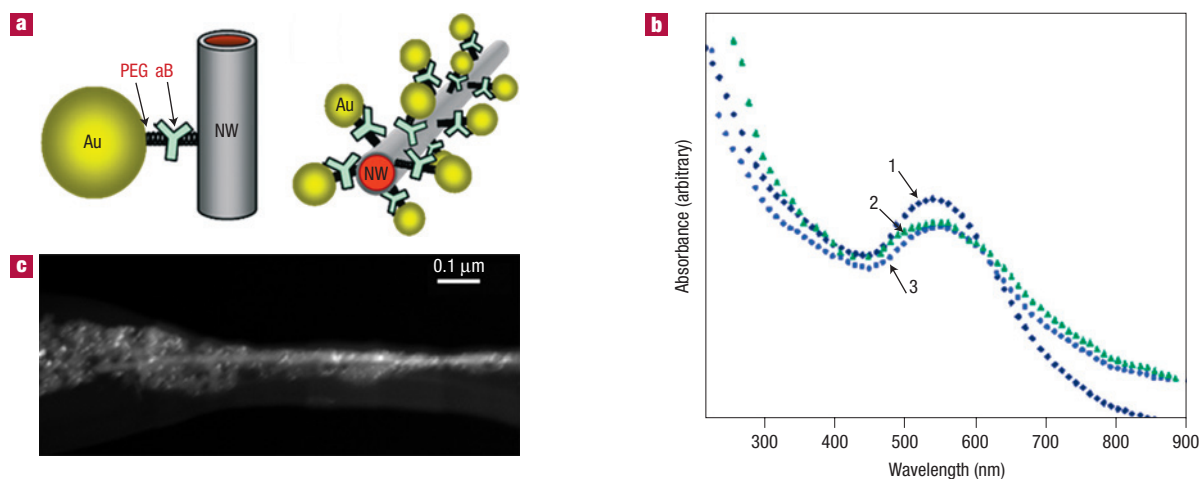


Figure 2 Preparation of NW-NP superstructures with PEG molecular springs. **a**, Schematic diagrams of MSA with Au NPs and CdTe NWs. The PEG molecules are expected to cover the entire surface of the NW. **b**, Absorption spectra of Au NPs at each conjugation step: 1, Au NP; 2, after attachment of PEG-aB complexes; 3, after the complete assembly of the MSA in **a**. **c**, Scanning TEM image of Au-PEG-aB-PEG-NW (the ratio of NP/NW was 5,000:1 in the conjugation step).

for further conjugation reactions with NPs and biomaterials²⁵. A 1-ethyl-3-(3-dimethylamino propyl) carbodiimide hydrochloride (EDC) crosslinking procedure can be used for the conjugation of this newly formed carboxylic group to any amine terminal²⁷.

The NW-NP MSA shown Fig. 2a was made by applying the above-described conjugation process twice. First, we made the NP-PEG-aB conjugate, then we attached this building block to a NW, producing an NP-PEG-aB-PEG-NW system (see the Methods section). The surface plasmon peak at 540 nm (Fig. 2b), characteristic of Au NPs, did not exhibit any spectral shift, except some broadening. This indicates that no agglomeration of Au NPs took place and that they remained as individual colloids. Considering the possibility of plasmon effects in Au clusters and the related field enhancement, it is clear that they do not play a significant role in the present system. The scanning transmission electron microscope (TEM) images confirmed the formation of the designed structure, where the two different nanomaterials were successfully linked together (Fig. 2c). Many Au NPs (bright dots) surround the CdTe NW, being embedded in the pale clouds attributed to the PEG chains.

Au NPs carrying PEG-aB segments were conjugated to construct superstructures with different ratios of NPs and NWs, denoted as NP5K, NP10K and NP20K. The starting solutions contained 5,000, 10,000 and 20,000 NPs per NW, respectively, and had different densities of Au NPs along the CdTe NWs, as can be seen in the scanning TEMs in the Supplementary Information. Note that in none of these superstructures did the particles form dense aggregates or exhibit a red-shift of the Au NPs absorption peak.

Conjugation using bifunctional PEG oligomers is important from several additional aspects. (1) PEG is one of the most flexible water-soluble polymers, which ensures the sensitivity of the MSA structure to the presence of analyte, that is, aG complementary to the aB incorporated in the MSA. (2) PEG chains are excellent agents for colloidal stabilization, which is important for proper optical behaviour. (3) PEGylated aBs have a long lifetime in solution²⁸. (4) PEG is also convenient for enhancing biological compatibility, which, although it may not be needed for many cases, is still a relevant property.

It was observed that the emission wavelength of the NP5K superstructure was blue-shifted by 8–10 nm (Fig. 3b, 1 → 2) during

the attachment of NPs to the NW, which was surprisingly similar to our expectations (Fig. 1b). When 20 μ l of SA was added, a red-shift of the luminescence spectra was observed (2 → 3 in Fig. 3b). This is also in complete agreement with the theoretical description above. The free SA forms an immunocomplex with the aB in the superstructure, which extends the molecular spring. Consequently, the exciton-plasmon interactions decrease, and so does γ_{NP} . This extends the time available for the exciton to diffuse along the NW and to find a site with lower energy, which produces the red-shift.

The advantage of using MSAs is the potential reversibility of the spectral processes in such structures, which is convenient both for sensing and validation of expected physical processes. To induce the reverse reaction, a certain amount, $\sim 10^4$ ng ml⁻¹, of unconjugated free aB was added to the media, which resulted in disruption of the SA-aB immunocomplexes in the MSA (Fig. 3) and recovery of the original superstructure. This procedure was repeated several times to show the reversibility of the emission wavelength shift. The reversibility was shown for two or three rounds of wavelength shifts, but the amplitude of the shifts gradually decreased owing to the progressive overloading of the solution with protein and potential photobleaching. NP10K and NP20K showed similar results with wavelength shifts of 6 and 9 nm on conjugation (1 → 2 process) and 5 and 2.5 nm for the addition of the same amount of SA (2 → 3 process), respectively. The high density of PEG in NP10K and NP20K probably prevents efficient formation of SA-aB complexes owing to steric frustration. In addition, the high density of the particles can accelerate exciton emission to the point where it no longer has time to diffuse, which reduces the wavelength shift.

It is important to demonstrate that the wavelength of emission depends on the concentration of the molecule of interest (Fig. 4). We therefore monitored the change in emission wavelength when different amounts of SA were added. The spectra were monitored for approximately 30–50 min until saturation, when the spectra stopped changing. The same experiments were conducted at each data point at least seven times. The wavelength of NW emission in NP5K was shifted within 2–10 nm with a monotonous increase for SA concentration between 10⁰ and 10⁵ ng ml⁻¹, which covers possible physiological concentration ranges for many different proteins. The generic version of the MSA must be tuned for the specific range of concentration by optimizing the NP density, NW-NP distance and the depth of the exciton traps in the NW. This

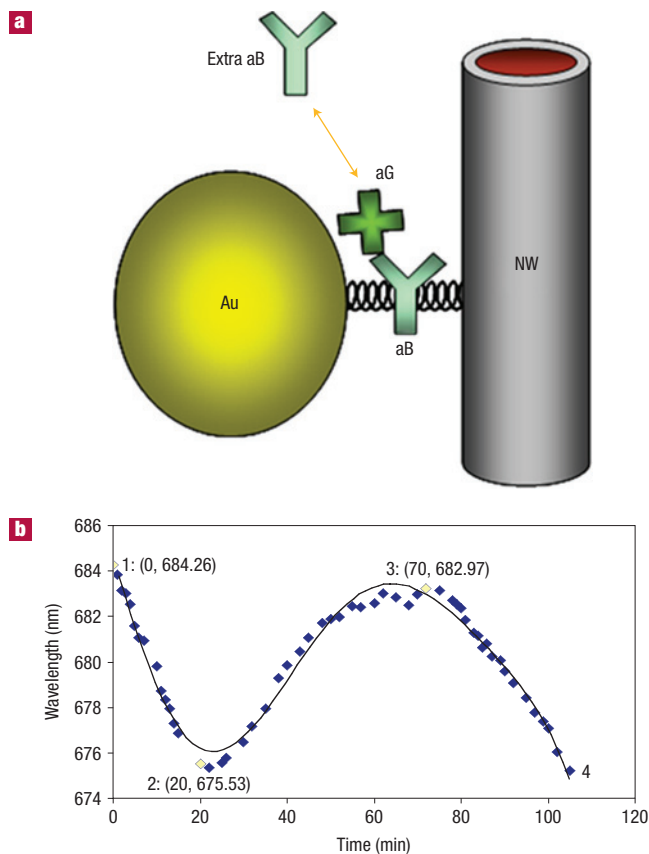


Figure 3 Wavelength shift in the NW-PEG-aB-PEG-NP superstructure. **a**, Schematic illustration of the aG-aB reaction in the MSA. The addition of extra amounts of aB will disrupt the aG-aB reaction in the NP-PEG-aB-PEG-NW superstructure. **b**, Reversible shift of the peak luminescence wavelength: 1, attachment of a NP to a NW; 2, after adding 20 μ l SA; 3, after adding free aB to the media; 4, after adding 20 μ l SA. Excitation wavelength: 420 nm.

will enable the creation of biosensors for desirable concentration ranges and will improve sensitivity.

In summary, the theoretically expected wavelength shift in an MSA of semiconductor NWs and metal NPs as a result of exciton-plasmon interactions and exciton dynamics was evaluated and confirmed through a series of experiments with structures comprising CdTe NWs and Au NPs. The wavelength shift occurs when exciton diffusion in NWs depends on the strength of the exciton-plasmon interactions, which are strongly dependent on the NW-NP distance. The insertion of an aB between the NP and the NW provides biological functionality to the superstructure and enables its use as a biosensor or an imaging contrast agent for conditions where the intensity readings are difficult to standardize. Most importantly, the range of the wavelength shift matches very well with the predicted data (Fig. 1b) for $\mu \approx 0.1\text{--}0.2 \text{ cm}^2 \text{ eV}^{-1} \text{ s}^{-1}$, which is a very reasonable estimate for the mobility of excitons in CdTe NWs in solution. This study provides a physical description of the processes in complex nanoscale systems and can serve as a firm foundation for further design of functional nanoassemblies. Compared with previous methods of sensing with Au and similar nanoparticles based predominantly on intensity variations^{4–6}, wavelength-shift MSAs can be particularly useful for biological applications, where the difference in the optical conditions of samples of heterogeneous tissues can be high. The concentration

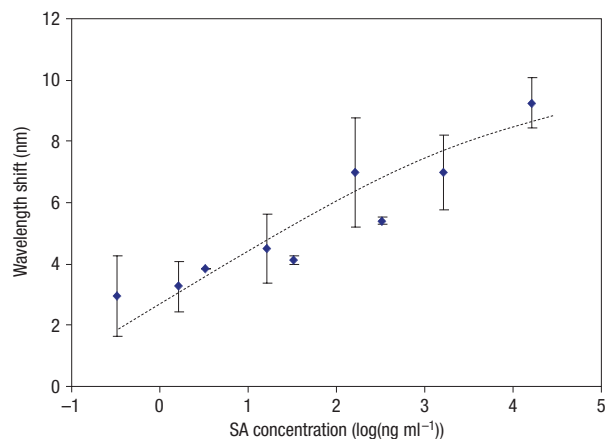


Figure 4 Calibration curve for SA. Averaged wavelength shifts for the hybrids in different analyte concentrations for 30–50 min until saturation of the wavelength shift. 20 μ l of SA from each buffer solution was added to 3 ml of PBS buffer (pH 7.2) in an optical cuvette for spectroscopic measurements. The molar ratios for the preparation of superstructures were determined from molar calculations for the nanocolloids. The concentrations of the NW and NP solutions were calculated to be $1.0 \times 10^{-9} \text{ M}$ and $4.5 \times 10^{-6} \text{ M}$ respectively on the basis of the physical dimensions of the particles and the synthesis data. The error bars represent the standard deviation in seven independent experiments. Excitation wavelength: 420 nm.

gradients of proteins are important in intercellular signalling, and the described nanostructures can significantly aid their detection and imaging. Unlike the shift in resonance absorption of Au NPs on clustering, the emission wavelength shows a clear gradual trend in response to the analyte concentration rather than discrete colourimetric readouts. Luminescence techniques always have greater sensitivity owing to the lower background. Compared with single-walled nanotube (SWNT) sensors based on wavelength shifts in near-infrared sensing of DNA²⁹, our superstructures are focused on proteins, which are (1) more ubiquitous than single-stranded DNA and (2) require greater distances in underlying electronic effects than what is typically afforded by donor-acceptor interactions owing to the physical size of proteins (a few nanometres). In addition, the emission of nanowires is more defined than that of SWNTs and can cover both the visible and infrared ranges of the spectrum. Note that the visible part is more convenient for imaging analyte maps inside, for instance, microfluidic or vascular devices than near-infrared owing to the simpler optics and better diffraction and aberration limits. Some disadvantages of NW-based sensors are that their endocytosis process has not been studied in as much detail as that for SWNT sensors, and localization and the actual fate of the NWs inside the cell can be different from that of SWNTs or NPs. A wider range of colloidal stability might be needed for both SWNTs and NWs.

METHODS

The synthesis of CdTe NWs from NPs has been described in detail elsewhere³⁰. Different CdTe NWs with diameters of $5.7 \text{ nm} \pm 1.3 \text{ nm}$, average longitudinal lengths of 400–1,200 nm and different photoluminescences at 684–710 nm in water were used to optimize the wavelength shifts. Au NPs were synthesized using Murray's method³⁰. The diameter of the NPs was measured to be 3.7 nm with a narrow size distribution using electron microscopy images obtained using a JEOL 2010F TEM.

The optimal protocol and reagent quantities to bind different nanomaterials are as follows: first, the surface of the Au NPs was functionalized

to obtain NH₂ functional groups by slight modification of methods to replace mercapto groups^{23,31,32}. A batch solution of cysteine, 1.3×10^{-3} M, was prepared. 100 μ l of this solution was added dropwise into 10 ml of Au NPs solution with stirring for 1 h, followed by stirring for more than 12 h to ensure complete reaction at the gold surface. Nanoparticles were purified by centrifugation and resuspension in water. Then 20 mg of NHS-CO-PEG-NH-*t*-BOC diluted in 700 μ l of water was added to this solution to allow conjugation to the surface of the Au NPs overnight with intermediate stirring. This procedure resulted in conjugation of the NHS terminus with the NH₂ group of the NP stabilizer via a covalent amide bond. After separation by ultracentrifugation and washing steps in PBS buffer (Sigma; biotechnology performance certified, pH 7.2), anti-SA was conjugated to the other end of the PEG molecule at room temperature for 1 h, after removing the *t*-BOC groups using 100 μ l of 10% trifluoroic acid for 20 min. The regenerated -NH₂ terminus of PEG can be conjugated to the C-terminus of anti-SA using standard conjugation techniques. The EDC method was used to link two functional groups. The EDC experimental procedure found in other publications^{12,25} was modified slightly to improve the stability of the Au NPs by dropping the EDC solution into the Au NPs solution with stirring. A fresh solution of 0.2 M EDC in 2 ml of PBS buffer was prepared at pH 7.2. The amount of EDC solution added was adjusted slightly according to the colour change and wavelength shift of the absorbance spectra of the Au NPs to avoid unwanted aggregation during the conjugation steps. Then, additional NHS-CO-PEG-NH-*t*-BOC conjugation on the NW was carried out using the same procedure as in the previous step. These solutions were then separated by ultracentrifugation to remove any remnants of unbound materials and stored at 4 °C until further conjugation and optical experiments. Ultraviolet-visible spectroscopic analysis was carried out to monitor the stability of the Au NPs. Immediately before the optical experiments, trifluoroic acid was added to remove *t*-BOC and to activate the carboxylic groups. EDC solutions were added, under vigorous stirring, using a syringe, resulting in covalent attachment of the CdTe NWs to the Au NP aB solution. Centrifugation, then redispersion of the precipitated pellet in PBS buffer (pH 7.2) was carried out for further optical experiments. 20 μ l of the superstructure solution was dispersed in a 3-ml-volume optical quartz cuvette with PBS buffer. The spectral change was monitored using a fluorescence photometer (Fluoromax-3, Jovin Yvon Horiba) at the excitation wavelength of 420 nm. The sizes of anti-SA, SA and PEGylated anti-SA were measured using a Zetasizer (Malvern).

Received 1 November 2006; accepted 16 February 2007; published 25 March 2007.

References

- Tang, Z. & Kotov, N. A. One-dimensional assemblies of nanoparticles: preparation, properties, and promise. *Adv. Mater.* **17**, 951–962 (2005).
- Zhang, J., Coombs, N., Kumacheva, E., Lin, Y. & Sargent, E. H. A new approach to hybrid polymer-metal and polymer-semiconductor particles. *Adv. Mater.* **14**, 1756–1759 (2002).
- Zhang, H. *et al.* Aligned two- and three-dimensional structures by directional freezing of polymers and nanoparticles. *Nature Mater.* **4**, 787–793 (2005).
- Niemeyer, C. M. Functional hybrid devices of proteins and inorganic nanoparticles. *Angew. Chem. Int. Edn* **42**, 5796–5800 (2003).
- Dyadyusha, L. *et al.* Quenching of CdSe quantum dot emission, a new approach for biosensing. *Chem. Commun.* 3201–3203 (2005).
- Oh, E. *et al.* Inhibition assay of biomolecules based on fluorescence resonance energy transfer (FRET) between quantum dots and gold nanoparticles. *J. Am. Chem. Soc.* **127**, 3270–3271 (2005).
- Fu, A. *et al.* Discrete nanostructures of quantum dots/Au with DNA. *J. Am. Chem. Soc.* **126**, 10832–10833 (2004).
- Gueroui, Z. & Libchaber, A. Single-molecule measurements of gold-quenched quantum dots. *Phys. Rev. Lett.* **93**, 166108 (2004).
- Lee, J., Govorov, A. O. & Kotov, N. A. Bioconjugated superstructures of CdTe nanowires and nanoparticles: Multistep cascade Foerster resonance energy transfer and energy channeling. *Nano Lett.* **5**, 2063–2069 (2005).
- Nikoobakht, B., Burda, C., Braun, M., Hun, M. & El-Sayed, M. A. The quenching of CdSe quantum dots photoluminescence by gold nanoparticles in solution. *Photochem. Photobiol.* **75**, 591–597 (2002).
- Sarathy, K. V., Thomas, P. J., Kulkarni, G. U. & Rao, C. N. R. Superlattices of metal and metal-semiconductor quantum dots obtained by layer-by-layer deposition of nanoparticle arrays. *J. Phys. Chem. B* **103**, 399–401 (1999).
- Lee, J., Govorov, A. O., Dulka, J. & Kotov, N. A. Bioconjugates of CdTe nanowires and Au nanoparticles: Plasmon-exciton interactions, luminescence enhancement, and collective effects. *Nano Lett.* **4**, 2323–2330 (2004).
- Dulkeith, E. *et al.* Fluorescence quenching of dye molecules near gold nanoparticles: Radiative and nonradiative effects. *Phys. Rev. Lett.* **89**, 203002 (2002).
- Ipe, B. I. & Thomas, K. G. Investigations on nanoparticle-chromophore and interchromophore interactions in pyrene-capped gold nanoparticles. *J. Phys. Chem. B* **108**, 13265–13272 (2004).
- Lakowicz, J. R. *et al.* Advances in surface-enhanced fluorescence. *J. Fluorescence* **14**, 425–441 (2004).
- Levin, C. S. *et al.* Chain-length-dependent vibrational resonances in alkanethiol self-assembled monolayers observed on plasmonic nanoparticle substrates. *Nano Lett.* **6**, 2617–2621 (2006).
- Kang, Y., Erickson, K. J. & Taton, T. A. Plasmonic nanoparticle chains via a morphological, sphere-to-string transition. *J. Am. Chem. Soc.* **127**, 13800–13801 (2005).
- Atwater, H. A., Maier, S., Polman, A., Dionne, J. A. & Sweatlock, L. The new p-n junction: Plasmonics enables photonic access to the nanoworld. *Mater. Res. Soc. Bull.* **30**, 385–389 (2005).
- Citrin, D. S. Coherent excitation transport in metal-nanoparticle chains. *Nano Lett.* **4**, 1561–1565 (2004).
- Wei, Q. H., Su, K. H., Durant, S. & Zhang, X. Plasmon resonance of finite one-dimensional Au nanoparticle chains. *Nano Lett.* **4**, 1067–1071 (2004).
- Wang, G. & Murray, R. W. Controlled assembly of monolayer-protected gold clusters by dissolved DNA. *Nano Lett.* **4**, 95–101 (2004).
- Maier, S. A. *et al.* Local detection of electromagnetic energy transport below the diffraction limit in metal nanoparticle plasmon waveguides. *Nature Mater.* **2**, 229–232 (2003).
- Chen, S. *et al.* Amperometric hydrogen peroxide biosensor based on the immobilization of horseradish peroxidase (HRP) on the layer-by-layer assembly films of gold colloidal nanoparticles and toluidine blue. *Electroanalysis* **18**, 471–477 (2006).
- Westenhoff, S. & Kotov, N. A. Quantum dot on a rope. *J. Am. Chem. Soc.* **124**, 2448–2449 (2002).
- Lee, J., Govorov, A. O. & Kotov, N. A. Nanoparticle assemblies with molecular springs: Nanoscale thermometer. *Angew. Chem. Int. Edn* **117**, 7605–7608 (2005).
- Govorov, A. O. *et al.* Exciton-plasmon interaction and hybrid excitons in semiconductor-metal nanoparticle assemblies. *Nano Lett.* **6**, 984–994 (2006).
- Yamamoto, Y. *et al.* Site-specific PEGylation of a lysine-deficient TNF- α with full bioactivity. *Nature Biotechnol.* **21**, 546–552 (2003).
- Chapman, A. P. PEGylated antibodies and antibody fragments for improved therapy: A review. *Adv. Drug Delivery Rev.* **54**, 531–545 (2002).
- Heller, D. A. *et al.* Optical detection of DNA conformational polymorphism on single-walled carbon nanotubes. *Science* **311**, 508–511 (2006).
- Jana, N. R., Gearheart, L. & Murphy, C. J. Seeding growth for size control of 5–40 nm diameter gold nanoparticles. *Langmuir* **17**, 6782–6786 (2001).
- Obare, S. O., Hollowell, R. E. & Murphy, C. J. Sensing strategy for lithium ion based on gold nanoparticles. *Langmuir* **18**, 10407–10410 (2002).
- Zhu, T., Vasilev, K., Kreiter, M., Mittler, S. & Knoll, W. Surface modification of citrate-reduced colloidal gold nanoparticles with 2-mercaptosuccinic acid. *Langmuir* **19**, 9518–9525 (2003).

Acknowledgements

The authors thank J. H. Bahng, Biomedical Engineering Department, University of Michigan, for useful discussion and assistance in biological experiments. The project was supported by NSF (N.A.K. and A.O.G.), DARPA, AFOSR, NIH (N.A.K.) and Ohio University (A.O.G.). Correspondence and requests for materials should be addressed to A.O.G. or N.A.K. Supplementary Information accompanies this paper on www.nature.com/naturematerials.

Author contributions

N.A.K. and J.L. carried out the experimental work and bio-assembly, whereas A.O.G. and P.H. carried out the theoretical study and modelling.

Competing financial interests

The authors declare no competing financial interests.

Reprints and permission information is available online at <http://npg.nature.com/reprintsandpermissions/>